Table 3. Electrophysiological Findings of Four Japanese Patients with KCNV2-retionpathy

Pt	DA 0.01		DA 30.0				Square shaped a-wave	Excessive enlargement of b-wave in the extended protocol	LA 3.0			LA 3.0 30Hz		
			A-wave		B-wave				A-wave	B-wave		B-wave		
	Amp (☒)	PT (ms)	Amp	PT	Amp	PT			Amp	PT	Amp	PT	Amp	PT
1	N	Del	N	Del	Super N	NA	(+)	(+)	Sub N	Del	Sub N	UD	UD	UD
2	UD	UD	N	Del	Super N	NA	(+)	NA	Sub N	Del	Sub N	Del	Sub N	Del
3	Sub N	Del	N	Del	Super N	N	(+)	NA	Sub N	Del	Sub N	Del	Sub N	N
4	Sub N	Del	N	Del	Super N	NA	(+)	(+)	Sub N	Del	Sub N	Del	Sub N	Del

Pt = patient; Amp = amplitude; PT = peak time; N = normal; UD = undetectable response; Sub N = subnormal; Del = delayed response; Super N=supernormal response; NA = not available. Full-field electroretinography (ERG) incorporating the standards of the International Society for Clinical Electrophysiology of Vision (ISCEV) included: (i) dark adapted dim flash 0.01 cd•s•m^{-2} (DA0.01), (ii) dark adapted bright flash 30.0 cd•s•m^{-2} (DA30.0), (iii) light adapted 3.0 cd•s•m^{-2} at 2 Hz (LA 3.0), and (iv) light adapted 3.0 cd•s•m^{-2} 30 Hz flicker (LA 3.0 30 Hz). The extended protocol also included the recording of dark adapted responses to an intensity series of flashes in order to detect an excessive enlargement of dark adapted b-wave (patients 1 and 4).

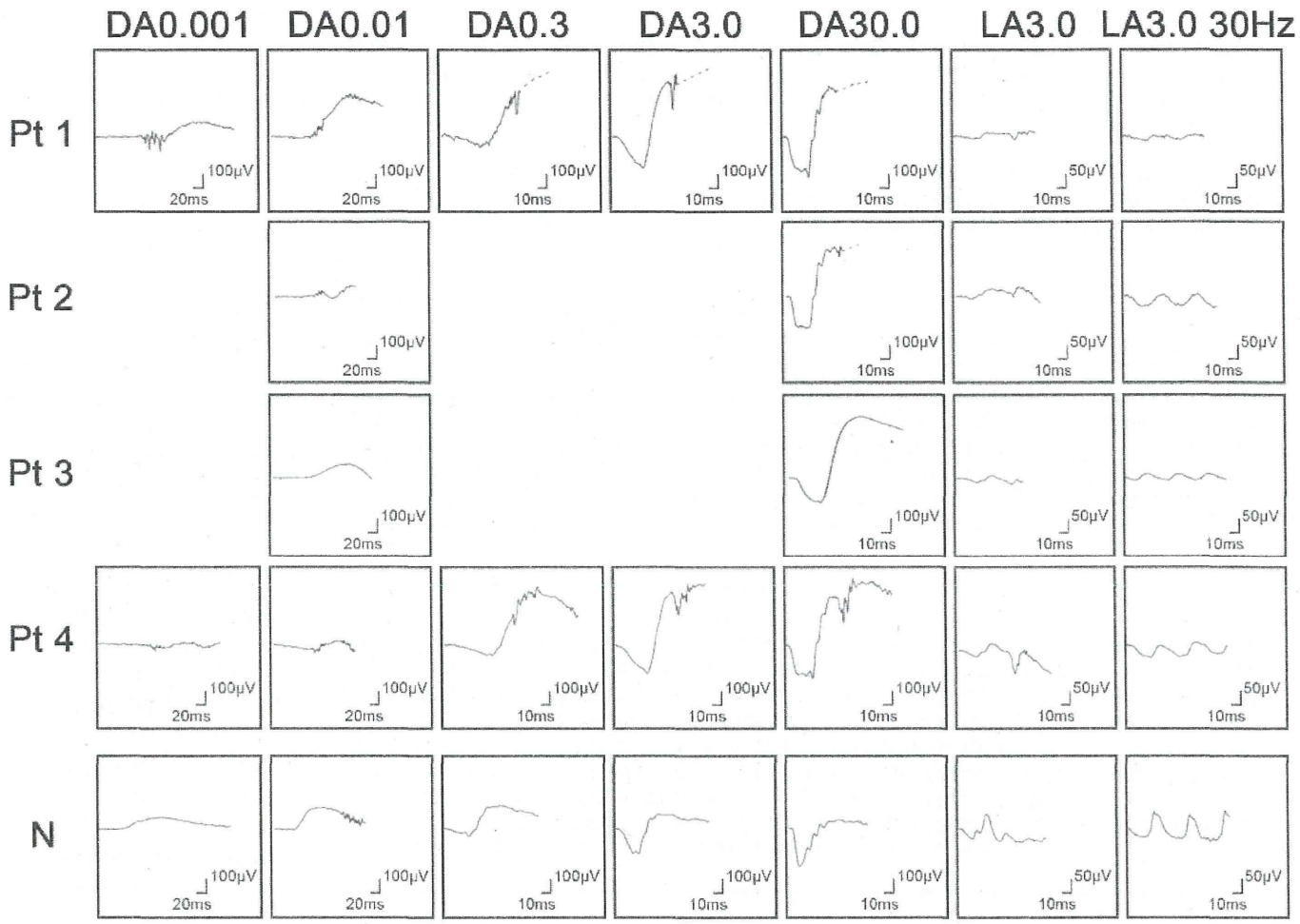

Figure 2. Electrophysiological findings of each patient with potassium channel, subfamily V, member 2 (*KCNV2*) retinopathy. Full-field electroretinograms (ERGs) of patient 1 (top row), patient 2 (second row), patient 3 (third row), and patient 4 (forth row) are shown. The ERGs from a normal control (bottom row) are also shown for comparison. All four patients underwent full-field ERG testing with the minimum standards of the International Society for Clinical Electrophysiology of Vision (ISCEV): (i) dark adapted dim flash 0.01 cd•s•m ^{2} (DA 0.01), (ii) dark adapted bright flash 30.0 cd•s•m ^{2} (DA 30.0), (iii) light adapted 3.0 cd•s•m ^{2} at 2 Hz (LA 3.0), and (iv) light adapted 3.0 cd•s•m ^{2} 30 Hz flicker ERG (LA 3.0 30Hz). The extended protocol was applied to two subjects (patients 1 and 4), including the recording of dark-adapted ERGs to an intensity series of flashes; 0.001 cd•s•m-^{2}, 0.01 cd•s•m ^{2}, 0.3 cd•s•m ^{2}, 3.0 cd•s•m ^{2}, and 30.0 cd•s•m ^{2}.

p.Arg206Pro, were not identified. Three missense variants, p.Arg27His, p.Cys177Arg, and p.Arg206Pro, were highly conserved among the orthologs, and one missense variant, p.Gly461Arg, was completely conserved (Figure 3).

A model of the *KCNV2* protein structure showing the approximate position of the missense disease-causing variants identified is presented in Figure 4. The KCNV2 protein comprises 545 amino acids and contains an N-terminal A and B box (NAB) and six transmembrane domains, (S1–S6), with a K selective motif, GlyTyrGly, in the pore-forming loop (P loop) between S5 and S6 [18]. One variant is located within the N-terminus (p.Arg27His), two variants, p.Cys177Arg and p.Arg206Pro, within the NAB, and one variant, p.Gly461Arg, within the P-loop.

Detailed molecular results of two non-disease-causing variants (polymorphisms) including the in silico analyses are summarized in Appendix 2. These two homozygous variants, p.Gly61Gly and p.Ala265Ala, were synonymous changes in the cording region and were predicted to be benign or have no effect on splicing (Polyphen2 and Human Splicing finder program analysis). Both were present in a high number of chromosomes in the Exome Variant Server database (7647/13006 for p.Gly61Gly and 5636/13006 for p.Ala265Ala, respectively).

Figure 3. Multiple alignment of eight species of potassium channel, subfamily V, member 2 orthologs. The amino acid-sequence alignment is numbered in accordance with the *Homo sapiens* potassium channel, subfamily V, member 2 (*KCNV2*) sequence (ENSP00000371514). The positions of mutated residues, Arg27 (c.8 G>A, p.Arg27His), Arg177 (c.529 T>C, p.Cys177Arg), Arg206 (c.617 G>C, p.Arg206Pro), and Gly461 (c.1381 G>A, p.Gly461Arg), are highlighted. The alignment was performed with the Clustal Omega program, and the asterisk indicates a completely conserved residue.

DISCUSSION

Our results showed the molecular genetic characteristics of four Japanese patients with CDSRR, which, to the best of our knowledge, is the first report of these characteristics of *KCNV2* retinopathy in an East Asian population. Our four patients harbored the likely disease-causing variants in *KCNV2*. Compound heterozygosity for two alleles, p.Cys177Arg and p.Gly461Arg, in three patients and homozygosity for two complex alleles, p.Arg27His and p.Arg206Pro, in one subject were confirmed. Three of the four variants, p.Arg27His, p.Cys177Arg, and p.Arg206Pro, were novel, which indicates all genotypes identified in our series have never been described before.

The clinical and electrophysiological characteristics of our four patients were similar to those of reported patients [8-11,13,14,17,18]. Additionally, all four patients presented with a decrease in central vision whose onset was in the first decade of life with minimal fundus changes and a characteristic ring enhancement of the AF signal (Table 2 and Figure 1). These findings are also in accordance with earlier reports [9-12,14]. SD-OCT demonstrated a discontinuous or absent inner and outer segment junction line in two patients

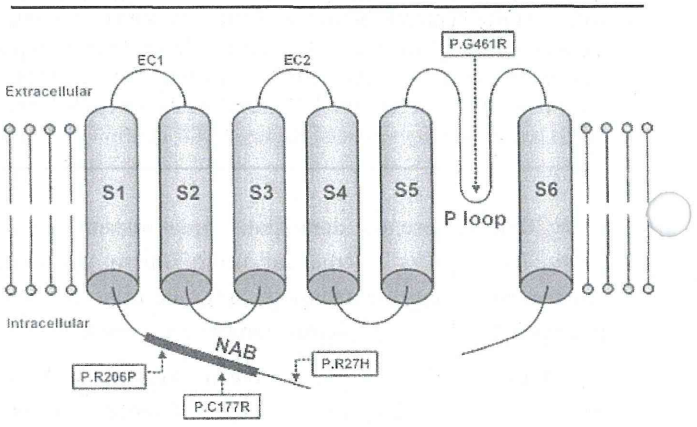

Figure 4. Model of the potassium channel, subfamily V, member 2 protein structure. A schematic representation of the potassium channel, subfamily V, member 2 (*KCNV2*) subunit of the K channel is drawn showing the approximate position of missense disease-causing variants identified in this study. The *KCNV2* protein consists of an N-terminus, an N-terminal A and B box (NAB), and six transmembrane domains (S1–S6), with two extracellular loops (EC 1, 2) and a K selective motif, GlyTyrGly, in the pore-forming loop (P loop) between S5 and S6.

as previously reported [10]. In addition, the absence of the cone outer segment tip line at the macular region was also confirmed in all four patients.

The pathognomonic electrophysiological features were demonstrated in all four patients, viz., delayed and reduced photopic ERGs, delayed ERGs for DA 0.01, and a square-shaped a-wave with a supernormal b-wave for DA 30.0 (Table 3 and Figure 2). An excessive increase in the b-wave for the DA ERGs to an intensity series of flashes was also confirmed in patients 2 and 3. Therefore, the unique rod system abnormalities were identical to those reported for *KCNV2* retinopathy [9,14].

Compound heterozygosity for two alleles, p.Cys177Arg and p.Gly461Arg, was found in patients 1, 2, and 3. The p.Gly461Arg with relatively higher allele frequency affects the third residue of the ultraconserved-GYG-tripeptide motif that acts as an ion selectivity filter in the K channel's pore-forming loop, P loop, between S5 and S6 (Figure 4) [30]. The clinical effect of p.Gly461Arg was well characterized earlier [10,16,17]. Friedburg et al. reported that three siblings with homozygous p.Gly461Arg had a relatively severe phenotype with an early onset and nystagmus at <5 years of age, visual acuity decrease (0.1–0.25, constantly), minimal fundus changes, ring enhancement at the foveal AF image, and an excessive increase in the b-wave for scotopic ERGs to an intensity series [17]. In contrast to the previous reports on homozygous patients, the three patients with heterozygous p.Gly461Arg in our series did not have nystagmus, and two of our patients had less severe BCVA decrease (0.7–0.8). These findings imply that the phenotype of the compound heterozygous for p.Gly461Arg and p Cys177Arg could have a less severe phenotype than those homozygous for p.Gly461Arg. It is of interest that the phenotypic spectrum, compound heterozygous for p.Gly461Arg and p Cys177Arg, was also observed in our series. Two relatively mild phenotypes were observed in the two siblings in our series (patients 1 and 2). In addition, one relatively severe phenotype, with more severe visual acuity decrease (0.1) and photoreceptor/RPE abnormalities at the macula, was detected in patient 3.

Three of the new disease-causing missense variants were located within the N-terminal region of the protein (Figure 4): p.Arg27His within the N-terminus and p.Cys177Arg and p.Arg206Pro within NAB. p.Cys177Arg was completely segregated, and the predicted pathogenesis and evolutionary conservation were confirmed. The coexistence of two likely disease-causing variants, p.Arg27His and p.Arg206Pro, on the same chromosome was also identified in our series with segregation analyses. The patient who was homozygous for these two complex variants had a severe phenotype, with an early onset (2 years), nystagmus, and severe visual acuity decrease (0.1 to 0.08). Both variants were predicted to be pathogenic with evolutionary high conservation (Appendix 1and Figure 3). Whether one of these variants is a neutral polymorphisms in cis with disease-causing one, or whether family 4's alleles are complex with two independently damaging missense variants remains to be determined.

To conclude, this study further delineates the molecular genetic findings of *KCNV2* retinopathy. Three putative novel variants were identified in our four Japanese patients with CDSRR, and our findings suggest there may be a distinct spectrum of *KCNV2* alleles in the Japanese population. However, the clinical findings were similar to that of the reported other population. Electrophysiology was fundamental to the diagnosis with pathognomonic findings due to channelopathy. The pathognomonic characteristics may be a useful method of determining the success of clinical therapeutic trials with gene replacement or pharmacological treatments for channelopathy.

APPENDIX 1. RESULTS OF IN SILICO MOLECULAR GENETIC ANALYSIS OF *KCNV2* MUTATIONS IDENTIFIED.

To access the data, click or select the words "Appendix 1." Pt = patient; Hom = homozygous; Het = heterozygous; SIFT = sorting Intolerant from Tolerance; HSF = human splicing finder program; CV = consensus values; EVS = exome variant server; POD = possibly damaging; PRD = probably damaging; ND = not detected. SIFT (version 4.0.4) results are reported to be tolerant if tolerance index ≥ 0.05 or intolerant if tolerance index < 0.05. Polyphen-2 (vision 2.1) appraises mutations qualitatively as Benign, Possibly Damaging or Probably Damaging based on the model's false positive rate. The cDNA is numbered according to Ensemble transcript ID ENST00000382082, in which +1 is the A of the translation start codon. Human splicing finder version 2.4.1 was applied to predict the effect of each variant on splicing. The results from HSF matrix indicate the values for the wild type and mutant sequences. The larger difference of values between the wild type and the mutant sequences indicates the greater change that the variant can affect on the splice site. EVS denotes variants in the Exome Variant Server, NHLBI Exome Sequencing Project, Seattle, WA.

APPENDIX 2. MOLECULAR ANALYSIS OF *KCNV2* POLYMORPHISMS.

To access the data, click or select the words "Appendix 2." Pt = patient; Hom = homozygous; Het = heterozygous; SIFT = sorting Intolerant from Tolerance; HSF = human splicing

finder program; CV = consensus values; EVS = exome variant server.

ACKNOWLEDGMENTS

We are grateful to the patients who kindly agreed to take part in this study and colleagues who referred individuals to us at National Institute of Sensory Organs. We thank Professor Duco I. Hamasaki (Bascom Palmer Eye Institute, Miami, FL) for proofreading. This research is supported in part by research grants from the Ministry of Health, Labor and Welfare, Japan and Grant-in-Aid for Scientific Research from JSPS.

REFERENCES

1. Gouras P, Eggers HM, MacKay CJ. Cone dystrophy, nyctalopia, and supernormal rod responses. A new retinal degeneration. Arch Ophthalmol 1983; 101:718-24. [PMID: 6601944].
2. Alexander KR, Fishman GA. Supernormal scotopic ERG in cone dystrophy. Br J Ophthalmol 1984; 68:69-78. [PMID: 6607068].
3. Yagasaki K, Miyake Y, Litao RE, Ichikawa K. Two cases of retinal degeneration with an unusual form of electroretinogram. Doc Ophthalmol 1986; 63:73-82. [PMID: 3015524].
4. Foerster MH, Kellner U, Wessing A. Cone dystrophy and supernormal dark-adapted b-waves in the electroretinogram. Graefes Arch Clin Exp Ophthalmol 1990; 228:116-9. [PMID: 2186970].
5. Kato M, Kobayashi R, Watanabe I. Cone dysfunction and supernormal scotopic electroretinogram with a high-intensity stimulus. A report of three cases. Doc Ophthalmol 1993; 84:71-81. [PMID: 8223112].
6. Rosenberg T, Simonsen SE. Retinal cone dysfunction of supernormal rod ERG type. Five new cases. Acta Ophthalmol (Copenh) 1993; 71:246-55. [PMID: 8333273].
7. Hood DC, Cideciyan AV, Halevy DA, Jacobson SG. Sites of disease action in a retinal dystrophy with supernormal and delayed rod electroretinogram b-waves. Vision Res 1996; 36:889-901. [PMID: 8736222].
8. Michaelides M, Holder GE, Webster AR, Hunt DM, Bird AC, Fitzke FW, Mollon JD, Moore AT. A detailed phenotypic study of "cone dystrophy with supernormal rod ERG". Br J Ophthalmol 2005; 89:332-9. [PMID: 15722315].
9. Robson AG, Webster AR, Michaelides M, Downes SM, Cowing JA, Hunt DM, Moore AT, Holder GE. "Cone Dystrophy with Supernormal Rod Electroretinogram": A Comprehensive Genotype/Phenotype Study Including Fundus Autofluorescence and Extensive Electrophysiology. Retina 2010; 30:51-62. [PMID: 19952985].
10. Sergouniotis PI, Holder GE, Robson AG, Michaelides M, Webster AR, Moore AT. High-resolution optical coherence tomography imaging in KCNV2 retinopathy. Br J Ophthalmol 2012; 96:213-7. [PMID: 21558291].
11. Vincent A, Robson AG, Holder GE. PATHOGNOMONIC (DIAGNOSTIC) ERGs A Review and Update. Retina 2013; 33:5-12. [PMID: 23263253].
12. Khan AO, Alrashed M, Alkuraya FS. 'Cone dystrophy with supranormal rod response' in children. Br J Ophthalmol 2012; 96:422-6. [PMID: 21900228].
13. Zobor D, Kohl S, Wissinger B, Zrenner E, Jagle H. Rod and Cone Function in Patients with KCNV2 Retinopathy. PLoS ONE 2012; 7:e46762-[PMID: 23077521].
14. Vincent A, Wright T, Garcia-Sanchez Y, Kisilak M, Campbell M, Westall C, Heon E. Phenotypic Characteristics including in vivo Cone Photoreceptor Mosaic in KCNV2-Related 'Cone Dystrophy with Supernormal Rod Electroretinogram'. Invest Ophthalmol Vis Sci 2013; 30:898-908. .
15. Tanimoto N, Usui T, Ichibe M, Takagi M, Hasegawa S, Abe H. PIII and derived PII analysis in a patient with retinal dysfunction with supernormal scotopic ERG. Doc Ophthalmol 2005; 110:219-26. [PMID: 16328930].
16. Wissinger B, Dangel S, Jagle H, Hansen L, Baumann B, Rudolph G, Wolf C, Bonin M, Koeppen K, Ladewig T, Kohl S, Zrenner E, Rosenberg T. Cone dystrophy with supernormal rod response is strictly associated with mutations in KCNV2. Invest Ophthalmol Vis Sci 2008; 49:751-7. [PMID: 18235024].
17. Friedburg C, Wissinger B, Schambeck M, Bonin M, Kohl S, Lorenz B. Long-term follow-up of the human phenotype in three siblings with cone dystrophy associated with a homozygous p.G461R mutation of KCNV2. Invest Ophthalmol Vis Sci 2011; 52:8621-9. [PMID: 21911584].
18. Wu H, Cowing JA, Michaelides M, Wilkie SE, Jeffery G, Jenkins SA, Mester V, Bird AC, Robson AG, Holder GE, Moore AT, Hunt DM, Webster AR. Mutations in the gene KCNV2 encoding a voltage-gated potassium channel subunit cause "cone dystrophy with supernormal rod electroretinogram" in humans. Am J Hum Genet 2006; 79:574-9. [PMID: 16909397].
19. Czirják G, Toth ZE, Enyedi P. Characterization of the heteromeric potassium channel formed by kv2.1 and the retinal subunit kv8.2 in Xenopus oocytes. J Neurophysiol 2007; 98:1213-22. [PMID: 17652418].
20. Hölter P, Kunst S, Wolloscheck T, Kelleher DK, Sticht C, Wolfrum U, Spessert R. The retinal clock drives the expression of Kcnv2, a channel essential for visual function and cone survival. Invest Ophthalmol Vis Sci 2012; 53:6947-54. [PMID: 22969075].
21. Beech DJ, Barnes S. Characterization of a voltage-gated K+ channel that accelerates the rod response to dim light. Neuron 1989; 3:573-81. [PMID: 2642011].
22. Thiagalingam S, McGee TL, Weleber RG, Sandberg MA, Trzupek KM, Berson EL, Dryja TP. Novel mutations in the KCNV2 gene in patients with cone dystrophy and a supernormal rod electroretinogram. Ophthalmic Genet 2007; 28:135-42. [PMID: 17896311].

23. Wissinger B, Schaich S, Baumann B, Bonin M, Jagle H, Friedburg C, Varsanyi B, Hoyng CB, Dollfus H, Heckenlively JR, Rosenberg T, Rudolph G, Kellner U, Salati R, Plomp A, De Baere E, Andrassi-Darida M, Sauer A, Wolf C, Zobor D, Bernd A, Leroy BP, Enyedi P, Cremers FP, Lorenz B, Zrenner E, Kohl S. Large deletions of the KCNV2 gene are common in patients with cone dystrophy with supernormal rod response. Hum Mutat 2011; 32:1398-406. [PMID: 21882291].

24. Nakamura N, Tsunoda K, Fujinami K, Shinoda K, Tomita K, Hatase T, Usui T, Akahori M, Iwata T, Miyake Y. Long-term Observation over Ten Years of Four Cases of Cone Dystrophy with Super-normal Rod Electroretinogram . Nippon Ganka Gakkai Zasshi 2013; In press.

25. Fujinami K, Tsunoda K, Hanazono G, Shinoda K, Ohde H, Miyake Y. Fundus autofluorescence in autosomal dominant occult macular dystrophy. Arch Ophthalmol 2011; 129:597-602. [PMID: 21555613].

26. Tsunoda K, Usui T, Hatase T, Yamai S, Fujinami K, Hanazono G, Shinoda K, Ohde H, Akahori M, Iwata T, Miyake Y. Clinical characteristics of occult macular dystrophy in family with mutation of Rp111 gene. Retina 2012; 32:1135-47. [PMID: 22466457].

27. Marmor MF, Fulton AB, Holder GE, Miyake Y, Brigell M, Bach M. ISCEV Standard for full-field clinical electroretinography (2008 update). Doc Ophthalmol 2009; 118:69-77. [PMID: 19030905].

28. Ng PC, Henikoff S. SIFT: Predicting amino acid changes that affect protein function. Nucleic Acids Res 2003; 31:3812-4. [PMID: 12824425].

29. Adzhubei IA, Schmidt S, Peshkin L, Ramensky VE, Gerasimova A, Bork P, Kondrashov AS, Sunyaev SR. A method and server for predicting damaging missense mutations. Nat Methods 2010; 7:248-9. [PMID: 20354512].

30. Heginbotham L, Lu Z, Abramson T, MacKinnon R. Mutations in the K+ channel signature sequence. Biophys J 1994; 66:1061-7. [PMID: 8038378].

Articles are provided courtesy of Emory University and the Zhongshan Ophthalmic Center, Sun Yat-sen University, P.R. China. The print version of this article was created on 20 July 2013. This reflects all typographical corrections and errata to the article through that date. Details of any changes may be found in the online version of the article.

Human Molecular Genetics, 2013, Vol. 22, No. 17 **3559–3567**
doi:10.1093/hmg/ddt210
Advance Access published on May 12, 2013

Enhanced optineurin E50K–TBK1 interaction evokes protein insolubility and initiates familial primary open-angle glaucoma

Yuriko Minegishi[1], Daisuke Iejima[1], Hiroaki Kobayashi[1], Zai-Long Chi[1], Kazuhide Kawase[2], Tetsuya Yamamoto[2], Tomohisa Seki[3], Shinsuke Yuasa[3], Keiichi Fukuda[3] and Takeshi Iwata[1,*]

[1]Division of Molecular and Cellular Biology, National Institute of Sensory Organs, National Hospital Organization Tokyo Medical Center, Tokyo, Japan [2]Department of Ophthalmology, Gifu University School of Medicine, Gifu, Japan [3]Department of Cardiology, Keio University School of Medicine, Tokyo, Japan

Received March 13, 2013; Revised April 15, 2013; Accepted May 1, 2013

Glaucoma is the leading cause for blindness affecting 60 million people worldwide. The optineurin (OPTN) E50K mutation was first identified in familial primary open-angle glaucoma (POAG), the onset of which is not associated with intraocular pressure (IOP) elevation, and is classified as normal-tension glaucoma (NTG). Optineurin (OPTN) is a multifunctional protein and its mutations are associated with neurodegenerative diseases such as POAG and amyotrophic lateral sclerosis (ALS). We have previously described an E50K mutation-carrying transgenic ($E50K^{-tg}$) mouse that exhibited glaucomatous phenotypes of decreased retinal ganglion cells (RGCs) and surrounding cell death at normal IOP. Further phenotypic analysis of these mice revealed persistent reactive gliosis and E50K mutant protein deposits in the outer plexiform layer (OPL). Over-expression of E50K in HEK293 cells indicated accumulation of insoluble OPTN in the endoplasmic reticulum (ER). This phenomenon was consistent with the results seen in neurons derived from induced pluripotent stem cells (iPSCs) from E50K mutation-carrying NTG patients. The E50K mutant strongly interacted with TANK-binding kinase 1 (TBK1), which prohibited the proper oligomerization and solubility of OPTN, both of which are important for OPTN intracellular transition. Treatment with a TBK1 inhibitor, BX795, abrogated the aberrant insolubility of the E50K mutant. Here, we delineated the intracellular dynamics of the endogenous E50K mutant protein for the first time and demonstrated how this mutation causes OPTN insolubility, in association with TBK1, to evoke POAG.

INTRODUCTION

Glaucoma is one of the world's leading cause of adult-onset blindness that causes optic nerve degeneration characterized by progressive and irreversible loss of retinal ganglion cells (RGCs) and retinal nerve fiber layer defects accompanied by the corresponding visual field damage (1). Open-angle glaucoma, the most prevalent subtype among various glaucomas, is further subdivided into two major types according to intraocular pressure (IOP). In the high-IOP type or primary open-angle glaucoma (POAG), elevated IOP due to disturbance of aqueous humor outflow in the trabecular meshwork or Schlemm's canal mechanically damages RGCs (2). In the normal-IOP type or normal-tension glaucoma (NTG), IOP elevation does not necessarily cause glaucoma, but some IOP-independent factors are thought to be involved (2). According to a population-based glaucoma survey conducted in Japan, NTG is the most prevalent subtype of glaucoma in the country (3, 4). This epidemiological study in Japan reported that the subjects' average IOP was ~15 mmHg and the POAG prevalence was almost equivalent in groups with IOP higher or lower than the average IOP (4). We have investigated the onset mechanism of the latter glaucoma subset, with lower IOP than average, as NTG. Interestingly enough, IOP-unrelated genetic mutations have been found recently in NTG (5, 6) and the Optineurin (OPTN) E50K mutation was the first one identified in familial NTG (7).

OPTN, a scaffold protein with various biological functions, has a few coiled-coil domains and a ubiquitin-binding domain

*To whom correspondence should be addressed at: Division of Molecular and Cellular Biology, National Institute of Sensory Organs, National Hospital Organization Tokyo Medical Center, 2-5-1 Higashigaoka, Meguro-ku, Tokyo 152-8902, Japan. Tel/Fax: +81 334111026; Email: iwatatakeshi@kankakuki.go.jp

at C-terminal. It associates with membrane trafficking proteins Myosin VI and Rab 8 to form Golgi ribbons and is involved in exocytosis (8, 9). And thus E50K mutation yields several phenotypes, such as fragmentation of Golgi apparatus (10), transport failure (8, 11) or apoptotic cell death (12, 13).

OPTN also participates in innate immunity response by regulating NF-κB activation and autophagy in anti-infection processes (14, 15) and via its interaction with some other proteins (16). Among the several OPTN mutations described in the original report, the role of a glutamic acid-to-lysine conversion at amino acid 50 (E50K) in NTG is well accepted worldwide (17–19). A family with a history of NTG was previously identified with the E50K mutation, and in affected members of this family, visual failure starts at about the age of 30 years (Supplementary Material, Fig. S1) and progresses to glaucoma without elevation of IOP until vision is entirely lost at about the age of 70 years (19). Recently, Maruyama *et al.* (20) identified three additional mutations in *OPTN*, a deletion in exon 5, a nonsense mutation (Q398X) and a missense mutation (E478G) that was associated with amyotrophic lateral sclerosis (ALS). Among these three mutations, the former two were recessive mutations and the latter E478G mutation was a dominant mutation, like E50K. The authors further showed the attenuation of the inhibitory effect of NF-κB activation by OPTN carrying the E478G mutation, but that the inhibitory function remained intact with the E50K mutation. Though the underlying causes of OPTN mutation-driven changes are different in POAG and ALS, it is still intriguing that OPTN plays crucial roles in neural homeostasis.

All these results suggest that the E50K mutant expression restricts retinal neural cell survival and is thus involved in the progression of POAG. The underlying molecular mechanism of how the glaucoma phenotype is evoked by a single amino acid replacement in OPTN is still unknown.

In this study, we further characterized the effects of the E50K mutation in OPTN in E50K transgenic ($E50K^{-tg}$) mice and explored the endogenous OPTN dynamics in neural cells differentiated from induced pluripotent stem cells (iPSCs) derived from NTG patients with the genetic mutation corresponding to E50K. At the molecular level, abnormal insolubility of the endogenous E50K OPTN mutant was demonstrated in this study for the first time. This insolubility was simultaneously attributed to the formation of a distinct protein complex, and to disabled oligomerization of OPTN, associated with an enhanced E50K–tank-binding kinase (TBK)1 interaction. The abnormal insolubility of the E50K mutant was rescued by treatment with a TBK1-specific inhibitor.

RESULTS

OPTN E50K transgenic mice exhibit profound gliosis in the retina

In our previous report, we showed that $E50K^{-tg}$ mice exhibited phenotypes, such as a decreased number of RGCs and progressive diminution of retinal thickness without elevation of IOP (19). Immunohistochemistry of the flat-mount retinas of $E50K^{-tg}$ mice showed persistent glial fibrillary acidic protein (GFAP)-positive dot-staining between astrocytes, compared with the staining pattern in retinas of wild-type mice (Fig. 1A and B). Evaluation of the pathological condition in age-matched wild-type and mutant mice by pathologists blinded to the sample source indicated significantly increased gliosis in the $E50K^{-tg}$ mice, compared with the wild-type mice (Fig. 1C). GFAP-positive Müller cells are known as one of the hallmarks for retinal neurodegenerative conditions, including glaucoma (21), which can be simulated by various retinal insults such as the optic nerve axonal damage, laser ablation and intravitreal injection of kainic acid (22–24). From the morphological analysis of the cells that appeared in the vertically incised retinal surface (Fig. 1D, dashed line), the GFAP-positive dots shown in the flat-mount specimen were concluded to be Müller cells, from their peculiar spindle shape (Fig. 1D, arrowheads). Reactive gliosis has been reported to be associated with retinal physical insults; thus, this phenotype in $E50K^{-tg}$ mice in the absence of physical insults was of particular interest. Therefore, in addition to the reactive gliosis in the retinas of $E50K^{-tg}$ mice, the retinal vessels were examined by *z*-axis confocal laser microscopy after tail vein injection of red fluorescent dye-conjugated isolectin. The confocal microscopy images revealed a number of gliosis scars embracing leakage of isolectin from vessels (Supplementary Material, Fig. S2A). These findings suggest that the retinas of $E50K^{-tg}$ mice are under continuous stress and are structurally vulnerable.

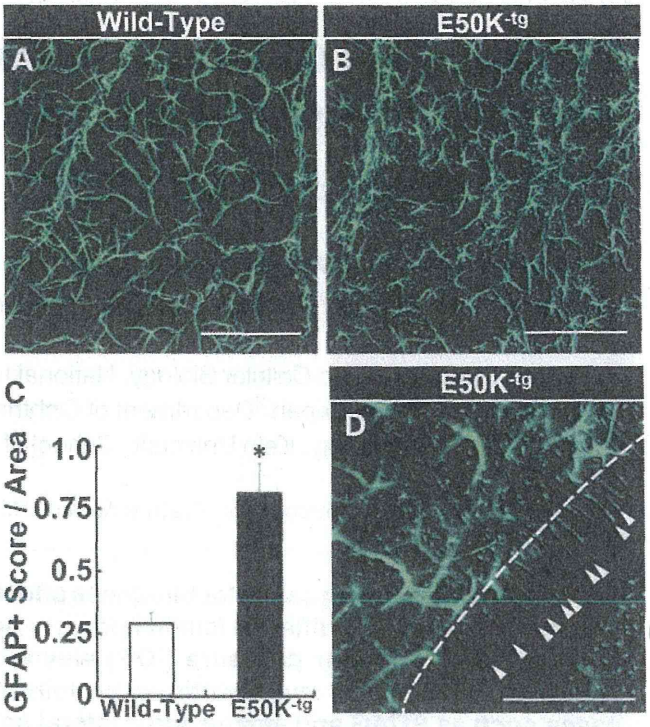

Figure 1. Persistent reactive gliosis in E50K-transgenic ($E50K^{-tg}$) mouse retinas. Representative retinal flat-mount immunohistochemistry images of anti-GFAP in (**A**) wild-type and (**B**) $E50K^{-tg}$ mice. Scale bar = 200 μm. Flat-mount specimens were analyzed (blinded evaluation) for gliosis assessment. The scores of GFAP-positive gliosis area/retinal area are plotted (data are mean ± SD; four fields of micrographs were chosen randomly and analyzed from one specimen, $n = 4$, $^*P < 0.05$). (**D**) The appearance of GFAP-positive Müller cells in $E50K^{-tg}$ mice. The dashed line indicates the border of the retinal luminal surface and the incised surface of the retina; arrowheads indicate the feet of GFAP-positive astrocytes. Scale bar = 100 μm. Some of the gliosis harbors the retinal vessel leakage (Supplementary Material, Fig. S1A).

OPTN E50K protein accumulates in the outer plexiform layer of the retinas of E50K^{-tg} mice

Considering the previous report of the deposit-like pathology in motor neurons in the ALS-associated OPTN E478G mutation (20), we also investigated the localization of the OPTN E50K protein in the retinas of E50K^{-tg} mice by immunohistochemistry. Negative control slides, treated with rabbit IgG cocktail alone, did not exhibit significant signals (Fig. 2A and B), while the retinas of E50K^{-tg} mice exhibited positive staining for OPTN in the outer plexiform layer (OPL) and the inner nuclear layer (INL), as small dot-like deposits (Fig. 2D and F, arrows). The retinas of wild-type littermates did not exhibit such a pattern (Fig. 2C and E). We designed this transgenic mouse with N-terminally HA-tagged OPTN protein, which would enable us to confirm whether the deposits include E50K mutant protein. HA-tagged E50K was mainly detected in the OPL of the retinas in E50K^{-tg} mice, which was consistent with the immunostaining results with the anti-OPTN antibody (Supplementary Material, Fig. S3D, arrows). Positive signals were not detected for OPTN in control slides in the retinas of wild-type mice and in those treated with the IgG alone (Supplementary Material, Fig. S3A–C). Thus, OPTN deposits in the retinas of E50K^{-tg} mice were caused exclusively from the expression of the E50K mutant. These pathology findings point to the capacity of the E50K mutant protein to aggregate.

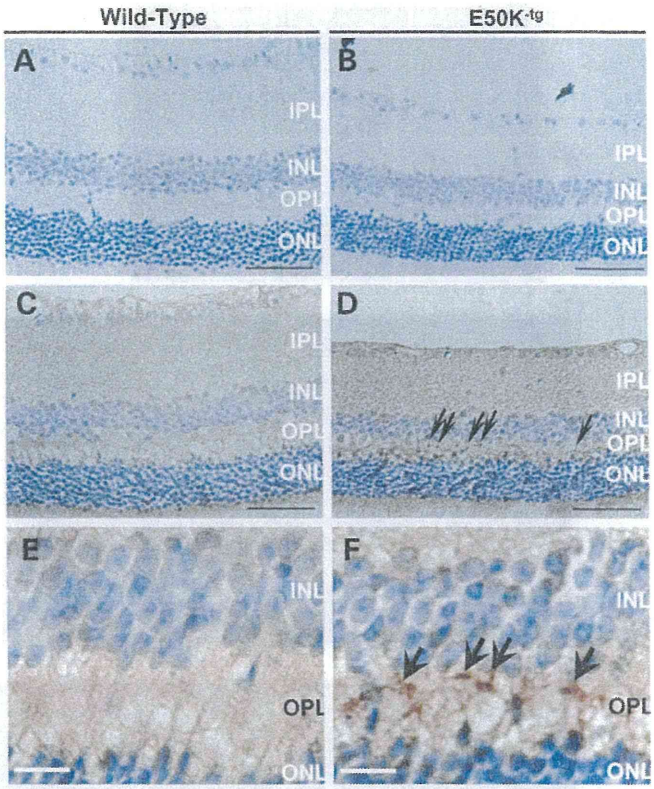

Figure 2. E50K mutant protein deposits in the retinas of E50K^{-tg} mice. (**A**) Rabbit IgG negative control for the immunohistochemistry analysis of the retina of a wild-type mouse. (**B**) Rabbit IgG negative control for the immunohistochemistry analysis of the retina of an E50K^{-tg} mouse. Both negative control slides showed minimum background staining. (**C**) Anti-OPTN immunohistochemistry of the wild-type mouse retina. Moderate OPTN signals were detected in luminal to inner layers of the retina. (**D**) Anti-OPTN immunohistochemistry of the E50K^{-tg} mouse. In addition to the moderate OPTN signals similar to that in the wild-type mouse retina, some strong deposit-like signals from INL to OPL were detected (indicated with arrows). Scale bars = 50 μm. High magnification micrograph of the retina of (**E**) wild-type and (**F**) E50K^{-tg} mice. Arrows indicate the OPTN deposit-like signals. Scale bars = 10 μm. The OPTN signals consists of, at least to some extent, the E50K^{-tg} transgene product, from the results of immunohistochemistry analysis with an anti-HA antibody (Supplementary Material, Fig. S2D). INL, inner nuclear layer; OPL, outer plexiform layer; ONL, outer nuclear layer.

Examination of induced neural cells from NTG patient-derived iPSCs indicates disturbed OPTN transition from ER to Golgi and Golgi body constriction

To clarify the cause of E50K mutant protein deposits in the retinas of E50K^{-tg} mice, we first examined the intracellular localization of wild-type OPTN and the E50K mutant by transfecting vectors encoding the two proteins fused with enhanced green fluorescent protein (EGFP) (^{EGFP}-OPTN and ^{EGFP}-E50K, respectively) into HEK 293 cells. ^{EGFP}-OPTN could be seen as small puncta widely distributed intracellularly, while ^{EGFP}-E50K was seen as larger puncta accumulated in the perinuclear region, and the Golgi body in the E50K-expressing cells was fragmented (Supplementary Material, Fig. S4B, arrowheads) as previously reported (10, 20). Since Golgi body formation and its membrane trafficking are associated with the endoplasmic reticulum (ER) (25, 26), ER structure was also examined using an ER detection kit (ER-ID, Enzo). Again, the wild-type OPTN was observed as small puncta dispersed within the cytosol (Fig. 3A), while the larger vesicles of the E50K mutant were accumulated in the perinuclear region surrounded by the ER membrane (Fig. 3B, arrows). To elucidate the intracellular localization of endogenous OPTN, we generated induced pluripotent stem cells (iPSCs) from peripheral blood mononuclear cells isolated from NTG patients with the mutation corresponding to E50K and examined OPTN localization in these cells. The pluripotency of iPSCs was confirmed by immunostaining with antibodies specific for Oct3 and Nanog, pluripotency markers (Supplementary Material, Fig. S5A). Neural induction was conducted as previously reported (27, 28) and neuronal differentiation was confirmed by staining with an antibody specific for Tuj1, a neuronal marker (Supplementary Material, Fig. S5B). iPSC-derived neural cells from NTG patients with the mutation corresponding to E50K were immunostained for OPTN and GM130, as a Golgi body marker, along with ER staining. In the iPSCs with wild-type OPTN, derived from a non-glaucoma subject, OPTN-associated vesicles were dispersed within the cells from ER to Golgi networks, in a pattern identical to that in HEK293 cells over-expressing wild-type OPTN (Fig. 3C). However, in the iPSCs from the NTG patient with the mutation corresponding to E50K, the number of OPTN-associated vesicles was decreased, compared with that in the control iPSCs, with dense aggregation in perinuclear regions and shrinkage of the ER/Golgi body (Fig. 3D). Upon microscopic examination under higher magnification, we found that wild-type OPTN frequently localized on the tips of Golgi ribbons (Fig. 3E), while the E50K OPTN mutant in iPSCs from NTG patients accumulated in the ER and Golgi body (Fig. 3F). Co-localization of wild-type OPTN and the Golgi body was

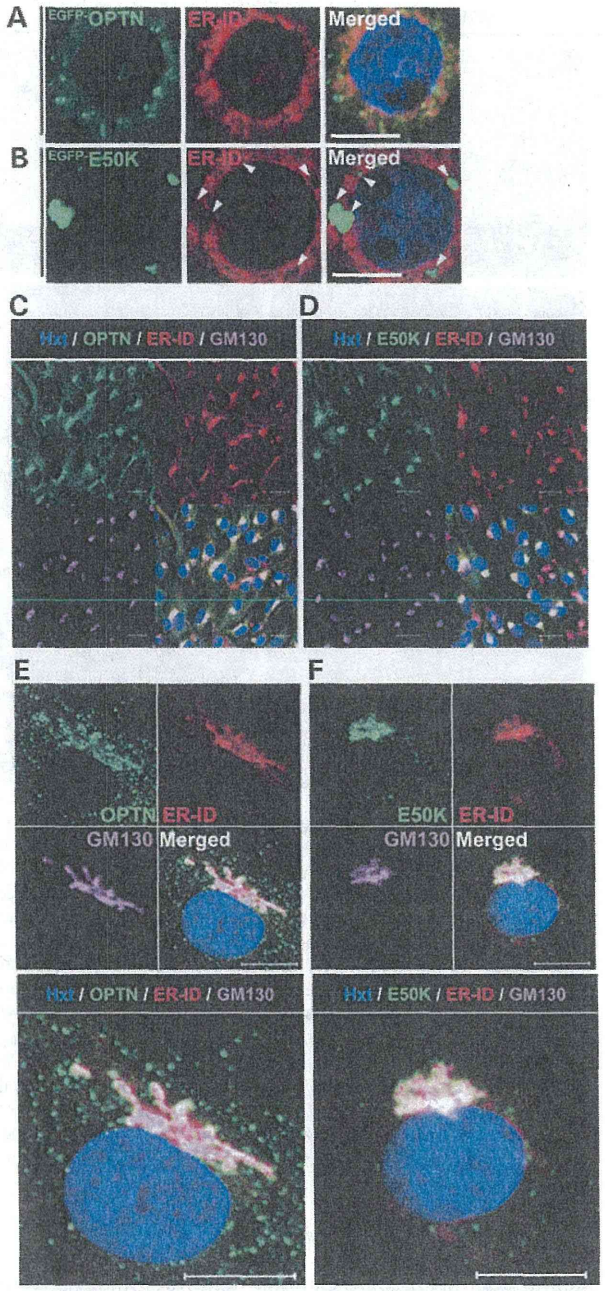

Figure 3. Distinct intracellular localization of wild-type OPTN and the E50K mutant. Intracellular localization of OPTN and E50K in over-expression studies. (**A**) ^{EGFP}-OPTN (green) and ER (red) localization 1 day after transfection. (**B**) ^{EGFP}-E50K mutant (green) and ER (red) localization 1 day after transfection. Both micrographs are shown with nuclear counter-staining with Hoechst 33342 (blue). Arrowheads indicate the E50K accumulation in the ER. Scale bars = 10 μm. iPSCs were established from iPSCs without the E50K mutation, derived from non-glaucoma subjects, as a control and with the E50K mutation, derived from glaucoma patients for endogenous analyses. Ten days after neural induction, OPTN (green), ER (red) and Golgi (magenta) co-localization were analyzed by immunocytochemistry. (**C**) Endogenous OPTN localization in neural control cells or (**D**) E50K glaucoma patient-derived neural cells. OPTN signals exhibited an accumulated pattern in cells with the E50K mutation. Higher magnification of endogenous OPTN signals in (**E**) control cells and (**F**) cells with the E50K mutation. In control cells, OPTN signals (green vesicles) were localized on the tips of ribbon Golgi body, while in the cells with the E50K mutation, the number of OPTN signals was decreased and largely accumulated within the ER and to a shrunken Golgi body (shown by the white signal in merged micrographs, respectively). All scale bars = 10 μm.

frequently observed (Supplementary Material, Fig. S4A, arrow), but such a co-localization was scarce for the E50K mutant (Supplementary Material, Fig. S4B). These results indicate that the expression of the E50K mutant affects OPTN transition from ER to Golgi body prior to Golgi shrinkage/fragmentation.

Insolubility of OPTN in iPSCs and iPSC-derived neural cells from NTG patients with the mutation corresponding to E50K

While performing the over-expression experiments, we noticed that the protein amount of over-expressed E50K was decreased to half that of wild-type OPTN in HEK293T cells. A similar result has been previously reported in dermal fibroblasts from the E50K mutation-carrying patients (29). Since there was no significant difference in the mRNA levels in both groups (Supplementary Material, Fig. S6A), we speculated that E50K is more susceptible to intracellular degradation. Our previous studies have shown that OPTN is degraded by proteasomal and lysosomal pathways (30). Therefore, we first treated cells with MG132, a proteasomal inhibitor, and bafilomycin, a lysosomal inhibitor, along with cycloheximide, a protein synthesis inhibitor, to compare the amount of protein degradation. The levels of over-expressed OPTN in cells treated only with cycloheximide were lower, while co-treatment with MG132 or bafilomycin restored the OPTN protein levels, as previously reported (Supplementary Material, Fig. S7A, OPTN lanes). However, over-expressed E50K mutant protein was not restored, unlike over-expressed wild-type OPTN, upon treatment of cells with inhibitors (Supplementary Material, Fig. S7A, E50K lanes). These results indicate that there was no association between the lower levels of the E50K mutant and intracellular degradation of OPTN. We predicted that E50K might be expressed at levels comparable to the wild-type protein, but was probably insoluble and was being precipitated with the insoluble pellet (Ppt.) fraction of the cell lysate after routine cell-lysate collection. Although an equivalent amount of calnexin, a Ppt. marker, was detected in the Ppt. fraction of both wild-type- and E50K-expressing HEK293 cells, ~2- to 5-fold higher amounts of E50K protein, compared with the wild-type OPTN, was detected in the Ppt. fraction (Fig. 4A and B). The insolubilized E50K increased in an E50K expression-dependent manner (Fig. 4C). To elucidate the reason for this altered solubility of E50K mutant protein, we utilized the aforementioned iPSCs and examined the OPTN protein levels by western blotting. Although the OPTN expression was moderate in undifferentiated iPSCs, OPTN was detected in the Sup. fraction of control iPSC lysates (Fig. 4D, control 1–4), while OPTN was detected in the Ppt. fraction of iPSCs from NTG patients with the mutation corresponding to E50K (Fig. 4D, E50K 1–6). OPTN expression was significantly increased after neural induction (Fig. 4E Sup. lanes). The iPSC-derived neural cells recapitulated these results, i.e. abundant OPTN in the Ppt. fraction in E50K mutation-carrying NTG patient-derived cells (Fig. 4E, Ppt. lanes). These findings indicate that regardless of the expression levels, the E50K mutant protein exhibits higher intracellular insolubility.